IEEE Access
Multidisciplinary | Rapid Review | Open Access Journal

Received 3 September 2022, accepted 5 October 2022, date of publication 10 October 2022, date of current version 17 October 2022.

Digital Object Identifier 10.1109/ACCESS.2022.3213698

RESEARCH ARTICLE

Evaluation of Aircraft Auxiliary Power Unit Near-Field Acoustics for Condition Monitoring

UMAIR AHMED, FAKHRE ALI, AND IAN K. JENNIONS
Integrated Vehicle Health Management Centre, School of Aerospace, Transport and Manufacturing, Cranfield University, MK43 0AL Bedfordshire, U.K.
Corresponding author: Umair Ahmed (umair.ahmed@cranfield.ac.uk)

This work was supported by the Boeing Company.

ABSTRACT This paper presents a comprehensive evaluation of the near-field acoustics of an aircraft auxiliary power unit (APU), based on experimental data acquired from an in-situ APU. The aim is to establish whether near-field acoustics can be implemented for online condition monitoring. The APU of Cranfield University's demonstrator aircraft, a Boeing 737-400, has been instrumented to acquire acoustics (near-field and far-field) and vibration data in synchronization with aircraft state parameters under a wide range of operating conditions. The acquired data is first implemented to determine the efficacy of employing near-field / far-field microphones, and vibration sensors, to monitor the combustion noise and tonal frequency levels from the APU components. Subsequently, an evaluation of the broadband characteristics of the vibroacoustic data and its variations against APU states and performance parameters is conducted based on several categories of feature extraction techniques. The findings suggest that nearfield acoustics lacks the ability to capture the combustion noise process. In addition, the tonal frequencies are also lost due to the level of background noise, fluctuations in the APU speeds, and scattering effects. For the same reasons, the phase couplings occurring between the signals generated by the APU components cannot be detected using acoustic data. Nevertheless, the overall analysis substantiates that the near-field acoustic data can be used to predict the APU operating states and has the potential to be implemented for developing APU performance parameter estimation models to enable condition monitoring.

INDEX TERMS Condition monitoring, acoustics, vibration, feature extraction, acoustic scattering, high order spectral analysis, coefficient of overlap, correlation coefficient, acoustic noise, aircraft.

I. INTRODUCTION

A. BACKGROUND

Monitoring of system parameters is essential for a feedback control system, ensuring system operation within the required performance and safety limits, and for condition monitoring purposes. The complexities associated with designing, integrating, and installing such a monitoring system depend primarily on the type of sensing mechanisms employed. Generally, the sensor required for a particular application depends on its capability to sense the desired variations in the system parameters or faults. The sensor-fault pairs (like vibration sensors for bearing faults, and pressure transducers for mass flow measurements) are well-established and are being used for a wide range of applications. However, the intrusive nature of most of these sensors can make them unsuitable for legacy aircraft due to hardware complexity and the associated cost, including certification, which escalates when developing retrofit solutions.

The aircraft auxiliary power unit (APU) is a turboshaft engine [1], composed of several rotating components, valves, guide vanes, igniters, and other associated accessories to generate the required electrical and pneumatic power for aircraft systems. An APU is a complex piece of machinery that requires continuous monitoring to ensure its performance and reliability. Due to accessibility issues, space, power, and weight constraints, installation of an elaborate sensor-set may be prohibitive, and the desired condition monitoring capability may not be possible. On the contrary, the acquisition of noise data using microphones may prove to be useful for such

The associate editor coordinating the review of this manuscript and approving it for publication was Yongming Li.

applications. A microphone-based solution could be readily deployed, non-intrusive, and cost-effective.

The authors have initiated research on the development of a microphone-based condition monitoring solution by first considering the far-field noise as a probable source of information about the health of the system. This led to the development of a far-field noise estimation model [2]. Sensitivity analysis has been performed using the developed model to quantify the effect of APU component degradation on the far-field noise. The effects, essentially negligible, have not led to any practical solution. Moreover, the solution employing far-field microphones is prone to interference from external effects and cannot be used for onboard condition monitoring. Therefore, in this study, the research has been extended to the near-field acoustic data to ascertain the feasibility of its utilization for onboard condition monitoring purposes.

B. LITERATURE REVIEW

Microphones have been used to study the sources of noise in the far-field of an aircraft APU. Coherence analysis is generally employed along with a set of multiple external and internal microphones to study the sources of direct and indirect combustion noise [3], [4]. The use of microphones is also common for noise measurements [5], its effect on airline employees [6], and the design of noise abatement solutions [7]. A recent study employed far-field microphone data to develop and validate a far-field noise estimation model for the complete range of APU operating conditions [2].

From the perspective of condition monitoring, microphones have been shown to detect faults in bearings, gears, and rotors using statistical features [8], [9], [10], frequency transform [11], [12], [13], [14], Bicoherence analysis [11], [14], spectral sub-bands [15] and symmetric dot patterns [16]. The proposed methodologies have been shown to be useful on individual components placed in a controlled environment to minimize acoustic reflections. The efficacy of these methods on an actual system in its original configuration is not known, and therefore the usual approach for condition monitoring of aircraft APUs is to use thermodynamic data acquired from a set of intrusive sensors [17].

The noise data acquired from a machine may also have broadband characteristics peculiar to the state in which the machine is operating. Several techniques can be used to transform broadband characteristics into useful features for further processing; such analysis has been widely used for speech-related applications. The use of Linear Predictive Coefficients (LPC) [18], [19], [20], [21], [22], [23] and spectral descriptors [24], [25], [26], [27] are among such applications. The same feature extraction techniques have not been evaluated on the noise generated by an aircraft APU and their usefulness for APU state and parameter estimation is yet to be ascertained.

C. SCOPE OF WORK

Although the use of microphones for condition monitoring purposes seems to be an attractive solution, the literature has been found to be lacking a detailed analysis of APU noise data (captured through microphones) to determine its potential utilization. In this research, a thorough examination of the noise generated by an in-situ aircraft APU is conducted in order to determine the usefulness of the microphone data for condition monitoring purposes. For this study, experimental data has been acquired from Cranfield University's Boeing 737-400 demonstrator aircraft [Section-II], which has been systematically processed using appropriate techniques [Section-III]. The results and discussion [Section-IV] present the scientific understanding associated with:

1) Detecting combustion noise along the periphery of the APU using microphones and vibration sensors.
2) The possibility of examining tonal frequencies generated by the APU components (shaft, gears, bearing) through acoustics.
3) Segregation between APU states using vibroacoustic (near-field microphones and vibration) sensors.
4) Establishing relationships between various features extracted from vibroacoustic data and APU thermodynamic parameters.

This paper is a precursor to a detailed study, which is being prepared, on the utilization of acoustics for condition monitoring of an aircraft auxiliary power unit. In the current paper the APU nearfield acoustic and vibration signatures, and their signal processing techniques, will be examined for application to condition monitoring. The findings of this paper are indicated where they occur {Finding #} and then referenced, in total, in the Conclusions. It is to be noted that, the primary focus of the paper is on analyzing the acoustic data, while the vibration sensor data is considered for comparison purposes.

II. BOEING 737-400 APU OPERATION

The Boeing 737-400 APU is a single-shaft gas turbine engine with a load compressor and a generator to support pneumatic and electrical loads (Fig. 1 in [2]). The APU has two centrifugal compressors (one for the power section and one for APU pneumatic system) with 17 impellers each, while the radial turbine has 14 blades. The APU operates at 63,830 rpm for all operating and load conditions. A set of Inlet Guide Vanes (IGVs) control the flow through the load compressor when demanded by the aircraft systems: the Environmental Control System (ECS), wing anti-icing, and the Main Engine Starter. A bleed valve (located outside the shroud) isolates the APU's output from the aircraft's pneumatic system and is put to a fully open position during bleed-on conditions. The surge control valve, controlled by the surge valve torque motor (SVTM), splits the flow produced by the load compressor towards the aircraft pneumatic system and the APU exhaust to prevent a surge condition.

The APU accessories (generator, fuel pump, cooling fan, and oil pump) are driven by the gearbox. Lubricating oil passes through the gearbox to reduce friction and gear wear. The oil temperature is regulated by an oil cooler which acts as a heat exchanger and the cooling air eventually leaves

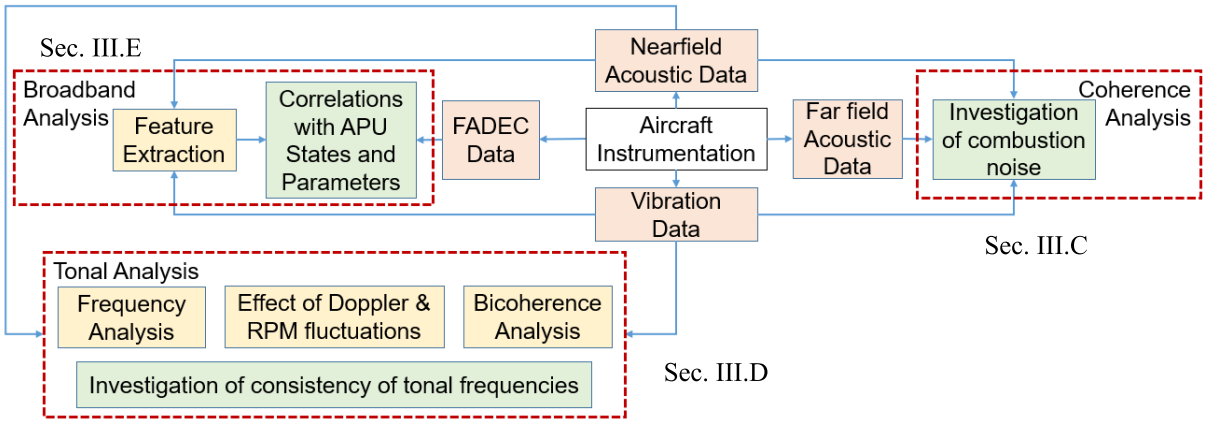

FIGURE 1. The scheme adopted for APU Acoustic Data Analysis.

the APU through the cooling air outlet. The APU assembly is enclosed inside a shroud for noise reduction and safety against fire. A Full Authority Digital Electronic Controller (FADEC) controls the APU operation by varying the IGVs, Surge Control Valve (SCV), and fuel flow to the combustor, based on the input from multiple sensors {RPM, Exhaust Gas Temperature (EGT), etc.} which can be viewed through the FADEC display.

The APU states can be divided into three categories:

1) Bleed system inactive (BL OFF)
2) Bleed System activated with no pneumatic load (BL ON NL)
3) Bleed System activated with pneumatic load (BL ON LD)

} BL ON

There are major variations taking place when the APU transitions from BL OFF to BL ON states and vice versa. In the latter state, the IGVs are fully open and there is a considerable rise in fuel flow. Whereas, between BL ON NL and BL ON LD, only mass flow through the bleed valve varies depending on the load. This is achieved by varying the SCV angles by changing the current through the SVTM, from 50mA for BL ON NL to a maximum of 95mA for BL ON LD conditions. The effects of load conditions on the APU thermodynamic parameters and the far-field noise have already been discussed [2].

III. ANALYSES PERFORMED

A. OVERVIEW

This paper systematically analyses the noise generated by an in-situ aircraft APU using appropriate signal processing techniques to address the research gaps found in the literature. The overall scheme adopted to perform the necessary set of analyses is presented in Fig. 1. Acoustic (far-field and near-field), Vibration and FADEC data form the basis of the analysis; these have been acquired from the aircraft APU in its original configuration (APU installed on vibration mounts with shroud and exhaust muffler). The complete analysis is divided into three categories:

(1) Coherence analysis between near-field and far-field noise to establish the existence of combustion noise inside the APU compartment.
(2) Tonal Frequency analysis evaluates the efficacy of utilizing near-field acoustic data for shaft, gearbox, and bearing condition monitoring. In this analysis, vibration data is treated as a reference and a comparison between the performance of commonly applied signal processing techniques using vibration and acoustic sensors has been carried out.
(3) Broadband noise analysis evaluates various features from the acquired vibroacoustic data for segregating between the APU states and utilizing them for APU parameter estimation.

B. EXPERIMENTAL DATA COLLECTION

The data collection is conducted by instrumenting Cranfield University's Boeing 737-400 aircraft APU. The overall experimental setup involved nine 130F20 1/4" IEPE microphones and 6 vibration sensors in combination with a National Instruments Data Acquisition (DAQ) System, allowing data sampling at 51.2 kHz. The arrangement of the microphones is illustrated in Fig. 2. Six microphones have been installed inside the APU shroud, while two (BV and BV2) were placed outside the shroud but within the APU compartment. The installation is made by attaching the microphones to the APU cables / wires that run across the APU. The naming convention adopted for the sensors allows quick identification of the sensor locations. The locations are chosen in such a way that the noise characteristics around the key APU components (BV, SCV, Oil Cooler, Combustor, Load Compressor) can be monitored. Moreover, the microphones have been placed uniformly to capture any trend in the acoustic characteristics across the APU compartment. One microphone is installed on the outside of the aircraft body (near the cooling air outlet) and is denoted by CAO. It will be utilized to study the effects of external noise sources on the near-field microphone data.

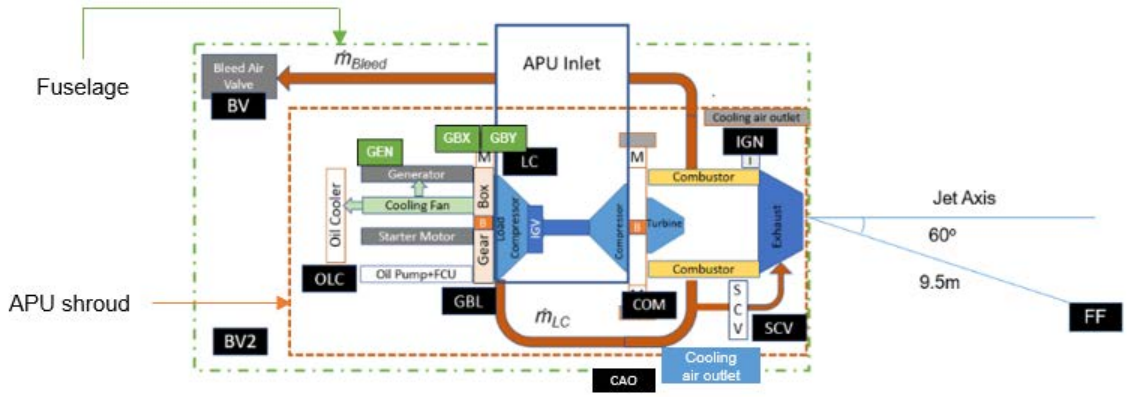

FIGURE 2. Microphone and vibration sensors placement.

Another microphone (FF) of the same specifications is placed in the far field of the exhaust. This microphone is on the left side of the jet axes so that the effect of noise from the APU inlet is minimized. The APU has also been instrumented with six CTC AC102 vibration sensors (using adhesive mounts) which have a dynamic range of 50g. These sensors are integrated with the same DAQ to ensure synchronized data acquisition. It should be noted that three out of the six vibration sensors did not provide readable data during the experimentation and were excluded from the analysis. For the remaining three sensors, sufficient data has been acquired, and only their locations are mentioned in Fig. 2. The setup also includes a camera facing the FADEC display for recording T_{Oil}, IGV angle, output pressure from the Load Compressor, and SVTM current. For mass flow through the bleed valve ($\dot{m}_{Bleed}$) and load compressor ($\dot{m}_{LC}$), appropriate relationships have been used, details of which have been previously reported [2]. The complete dataset was acquired over a period of five months.

C. NEAR-FIELD AND FAR-FIELD NOISE COHERENCE ANALYSIS

Combustion noise levels can provide useful information about the state and health of an APU. These levels can be measured in the far-field of the APU exhaust due to the distinct nature of the combustion spectra at lower frequencies [2], [28], [29]. Moreover, they can also be predicted by using semi-empirical relationships, with APU geometric and thermodynamic data [30]. For exact measurements, highly specialized acoustic sensors have to be installed intrusive in the combustor to withstand the harsh environment. To avoid hardware complexities associated with the intrusive sensors, it is desired that have the same information using ordinary measurement microphones.

To detect the presence of combustion noise along the periphery of the APU structure, coherence analysis has been performed to ascertain the extent to which the low frequency (combustion) noise is related between the far-field and near-field acoustic / vibration sensors. The analysis also establishes a relationship (if any) between the tonal noise components of the far-field microphones and the vibration sensor. MATLAB's '*mscohere*' function has been utilized for this analysis with a window size of 51200 samples (1 second) with 95% overlap and an FFT size of 218. The resultant magnitude- squared (Mag. Sq.) coherence estimate is in the range [0,1] for each of the frequency bins, where a value of 1 at a certain frequency indicates a linear relationship, and nonlinear otherwise. The analysis has been done separately for BL OFF and BL ON to evaluate the effect of activation of the APU's pneumatic system on coherence.

D. TONAL ANALYSIS

The use of vibration sensors for observing the tonal frequencies generated by a gas turbine (or an APU) for condition monitoring purposes has been well-established and is widely employed. The amplitude and the location of the tones generated by shafts, bearing, and gearbox can be used for fault detection and identification. For example, the amplitude of the sidebands in the gear mesh frequency corresponds to the gear tooth breakage [31] for a gearbox. During the early stages of the fault, the sideband amplitudes are very low and are further deteriorated by the background noise. The situation may become worse if acoustic sensors are employed due to the increase in the background noise levels. For accurate results, the signal (or tonal) amplitudes should be higher than the noise levels (i.e., high SNR), so that they are observable in the frequency domain.

In this study, the efficacy of utilizing microphones for monitoring tonal frequencies is established. Since faults have not been injected into the aircraft APU due to operational and safety concerns, the vibration data is treated as a reference. The exact source of the tones is also not discussed, due to the unavailability of the gearbox / bearing geometry details which are proprietary to the OEM. The aim is to determine the extent to which the acoustic sensors can capture the same number of tonal frequencies which are being captured by the vibration sensors.

First, coherence between a vibration sensor and the near-field microphones is carried out to determine the possibility of acquiring the tonal frequencies using either of the sensing mechanisms. The coherence estimates have been computed in the same manner as mentioned in section III.C while considering one of the three installed vibration sensors as a reference. In the analysis, each microphone has been treated separately to identify the locations where a greater number of coherent tones can be acquired. The effect of change in the APU load conditions on the tonal amplitudes and overall noise levels is also discussed, and the possible explanation for such variations is presented. Lastly, the usefulness of Bicoherence analysis on acoustic data using experimental and simulated data is presented.

E. BROADBAND NOISE ANALYSIS

In this analysis, the vibroacoustic response with the variation in APU states and parameters is studied. This analysis aims to determine the usefulness of using nearfield acoustic and vibration data for APU state identification and parameter estimation. To achieve this, several feature extraction techniques are employed on the vibroacoustic data, and the performance of the resultant features is evaluated against a defined performance metric. Comparison between the performance of acoustic and vibration data is an inherent part of the analysis. This analysis comprises the description of the various categories of features employed, performance analysis of features against different APU states using the coefficient of overlap as a metric, and lastly, studying the correlation of the features with various APU parameters.

1) DATA PREPARATION AND FEATURE EXTRACTION

For computing the requisite sets of features, the time series data from the vibroacoustic sensors is divided into segments of one second with 80% overlap. For each segment, five different categories of features are computed, which are:

(a) A set of 20 linear predictor coefficients (LPC) with the error term, which are computed using MATLAB '*lpc*' function.
(b) Mel-Frequency Cepstral Coefficients (MFCC), keeping the 20 triangular filters regularly spaced between 0 and 25.6kHz.
(c) Spectral Power in sub-bands (BandPower) corresponding to the average power in the 20 sub-bands computed using MATLAB's '*bandpower*' function.
(d) The time-domain feature set includes RMS, Kurtosis, Skewness, Max, Zero Crossing Rate, Negentropy [32, eq. (81)], Impulse Factor, Crest Factor, and the Shape Factor.
(e) Spectral Descriptors include the characteristics derived from the audio frequency spectrum. These are computed using the audio signal processing toolbox in MATLAB and include skewness, spread, centroid, flatness, arithmetic mean, geometric mean, crest, spectral peak, flux, slope, decrease, and roll-off point.

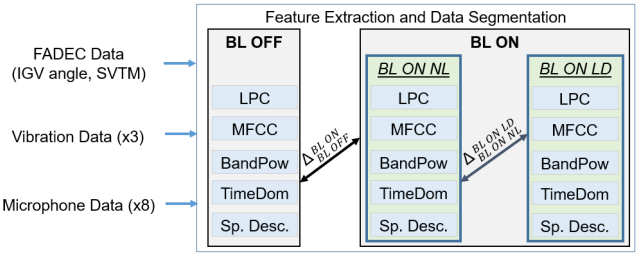

FIGURE 3. Process followed for analyzing feature response under the various APU States.

The thermodynamic parameters corresponding to the data segments are also noted, and the segments are labeled as per the APU states:

$$\begin{aligned} \text{BL OFF} &\rightarrow \text{IGV angle} = 22 \\ \text{BL ON NL} &\rightarrow \text{IGV angle} > 22 \text{ and SVTM} = 50 \\ \text{BL ON LD} &\rightarrow \text{IGV angle} > 22 \text{ and SVTM} > 50. \end{aligned}$$

2) EVALUATION OF FEATURE RESPONSE AGAINST THE APU STATES

From the perspective of condition monitoring, it is important to ascertain the current state in which the APU is operating. Any disparity between the current and the desired state of operation can indicate the presence of a faulty condition. In this study, the features extracted from the vibroacoustic data have been evaluated to ascertain the potential of the use of microphones and vibration sensors for condition monitoring purposes. The overall approach followed is presented in Fig 3. The five different categories of features are computed for the vibroacoustic data using the approach mentioned in section III.E.1. The computed features are then segregated into three categories depending on the APU State determined from the FADEC Data. For each of the features, coefficients of overlap ($\Delta^{BL\ ON}_{BL\ OFF}$ and $\Delta^{BL\ ON\ LD}_{BL\ ON\ NL}$) [33] are then computed to evaluate performance, where:

$$\Delta^{BL\ ON}_{BL\ OFF} = \int min\left\{f_{BL\ OFF}(x),\quad f_{BL\ ON}(x)\right\} dx \qquad (1)$$

and:

$$\Delta^{BL\ ON\ LD}_{BL\ ON\ NL} = \int min\left\{f_{BL\ ON\ NL}(x),\quad f_{BL\ ON\ LD}(x)\right\} dx \qquad (2)$$

In the above equations, $f_{BL\ OFF}(x)$, $f_{BL\ ON}(x)$, $f_{BL\ ON\ NL}(x)$, *and* $f_{BL\ ON\ LD}(x)$ correspond to the probability density functions of a feature for BL OFF, BL ON, BL ON NL, and BL ON LD conditions respectively. MATLAB's '*ksdensity*' function has been used to estimate the probability density function of a feature for a particular APU state, and '*trapz*' function is employed to perform the required numerical integration after the '*min*' operation. The values of the coefficient of overlap for a particular feature can range between [0,1],

with lower values indicating that the feature changes significantly between different APU states, thus leading to a lower overlap between the feature values between those two states. This would be a desirable condition, as opposed to a situation in which the feature values do not alter significantly even if the states are changing.

The values of $\Delta_{BL\ OFF}^{BL\ ON}$ and $\Delta_{BL\ ON\ NL}^{BL\ ON\ LD}$ have been segregated into the type of sensor used (acoustic / vibration) against each feature category. The resultant dataset contains 20 vectors: Two coefficients of overlap ($\Delta_{BL\ OFF}^{BL\ ON}$ and $\Delta_{BL\ ON\ NL}^{BL\ ON\ LD}$), two types of sensors (acoustics and vibration) and five categories of features (LPC, MFCC, BandPower, TimeDomain and Spectral Descriptors). The resultant dataset is labeled as follows:

$$\left[\Delta_{BL\ OFF}^{BL\ ON}, \Delta_{BL\ ON\ NL}^{BL\ ON\ LD}\right]_{Acoustic, Vibration}^{LPC,\ MFCC,\ BandPower,\ TimeDomain,\ SpectralDescriptors} \tag{3}$$

The subscript refers to the sensor type, while the superscript represents the feature extraction technique used for each category of the sensor. For example, $\left[\Delta_{BL\ OFF}^{BL\ ON}\right]_{Acoustic}^{MFCC}$ is a vector comprising 160 values of coefficients of overlap between BL OFF and BL ON conditions corresponding to each of the 20 MFCC features for all eight microphones:

$$\left[\Delta_{BL\ OFF}^{BL\ ON}\right]_{Acoustic}^{MFCC} = [\ \Delta_{BL\ OFF_{S1}}^{BL\ ON^{MFCC1}} \ \ldots\ \Delta_{BL\ OFF_{S1}}^{BL\ ON^{MFCC20}} \ \ldots\ \Delta_{BL\ OFF_{S8}}^{BL\ ON^{MFCC1}} \ \ldots\ \Delta_{BL\ OFF_{S8}}^{BL\ ON^{MFCC20}}]$$

Here, $S1 - S8$ correspond to eight of the microphone locations, and $MFCC1 - MFCC20$ are the 20 MFCC features computed at each of those sensor locations The distributions of the resultant dataset (expression 3) are eventually analyzed to ascertain the potential of using vibroacoustic data for the desired condition monitoring purposes.

3) FEATURES' RESPONSE WITH APU PARAMETERS

Continuous monitoring of APU parameters, like mass flows, oil temperatures, and IGV angles, can also give insight into the health of the system. Generally, several intrusive sensors are employed, however, in this study, the capability of using microphones for the same purpose is explored. The results are also compared with that of using vibration sensors. Similar to the process followed in section III.E.2, the variation in the feature responses to the various APU parameters is analyzed. The correlation coefficient (ρ) is utilized to act as a metric to establish a relationship (if any) between an APU parameter (P) and a feature (F) for a specific sensor (S_i):

$$\rho_{P_{Si}^{F}} = \frac{1}{N-1}\sum_{i=1}^{N}\left(\frac{F_i - \mu_F}{\sigma_F}\right)\left(\frac{P_i - \mu_P}{\sigma_P}\right) \tag{4}$$

where 'N' is the number of datapoints, 'F_i' and 'P_i' are the feature and the parameter values at datapoint 'i', and σ and μ represent the standard deviation and mean. Four of the APU parameters are considered, which include $\dot{m}_{Bleed}$, $\dot{m}_{LC}$, IGV angles, and T_{Oil}. By observing these parameters, the state of APU pneumatic system components (IGVs, SCV, and BV) and lubrication oil cooling system can be monitored, and deviations from the nominal limits will indicate the presence of a faulty condition. The result of this analysis is a dataset containing 40 vectors comprising four sets of correlation coefficients corresponding to the four APU parameters, two types of sensors, and five categories of features:

$$[\rho_{TOil}, \rho_{mLC}, \rho_{IGV}, \rho_{mBleed}]_{Acoustic, Vibration}^{LPC,\ MFCC,\ BandPower,\ TimeDomain,\ Spectral\ Descriptors} \tag{5}$$

As an example, $[\rho_{TOil}]_{Acoustic}^{LPC}$ is a vector containing 168 values corresponding to the correlation coefficients between each of the 21 features from eight microphones and T_{Oil}, that is,

$$[\rho_{TOil}]_{Acoustic}^{LPC} = [\ \rho_{TOil_{S1}}^{LPC1} \ldots \rho_{TOil_{S1}}^{LPC21} \ldots \rho_{TOil_{S8}}^{LPC1} \ldots \rho_{TOil_{S8}}^{LPC21}]$$

Here, $S1 - S8$ corresponds to eight of the microphone locations, and $LPC1 - LPC21$ are the 21 LCP features computed at each of those sensor locations. In this study, the distributions of each of the 40 vectors ($[\rho_{TOil}]_{Acoustic}^{LPC}$, $[\rho_{mLC}]_{Acoustic}^{MFCC}$, $[\rho_{mBleed}]_{Vibration}^{BandPower}$, etc) are visualized to assess the range of correlation values existing between features and APU parameters for acoustic and vibration sensors.

It is to be noted that, since the IGV angles are only modulating during BL ON states, the correlation coefficients for the IGV angles have been computed for those durations only. Similarly, the correlation coefficients for $\dot{m}_{Bleed}$ include the data from BL ON LD state only because it is zero otherwise. Whereas, for Toil and $\dot{m}_{LC}$, the data from all the states have been considered.

IV. RESULTS AND DISCUSSION

This section presents a detailed picture of the three independent analyses that have been performed on the APU noise. Initially, the coherence analysis between the far field and nearfield acoustic is presented. This is followed by the analysis of the tones present in the acquired vibration and acoustic data. The disparity between the results is then explained using engineering and physics principles. The practicality of using Bicoherence analysis on APU acoustic data is also presented, and validation of the results is done using synthetically generated data. Lastly, a thorough analysis of several features extracted from the vibroacoustic data is carried out and the results of coefficients of overlap and correlation coefficients are presented in a summarized form.

A. NEAR-FIELD AND FAR-FIELD NOISE COHERENCE ANALYSIS

Coherence estimates have been computed by choosing the far-field microphone as a reference using 20 seconds of data, and the results are presented in Fig. 4. Apart from the outside shroud sensors (BV and BV2), there is a common trend for all the sensors. Only a few tones [generator shaft rpm of 100Hz, shaft frequency of 1 kHz and its harmonics, and compressor

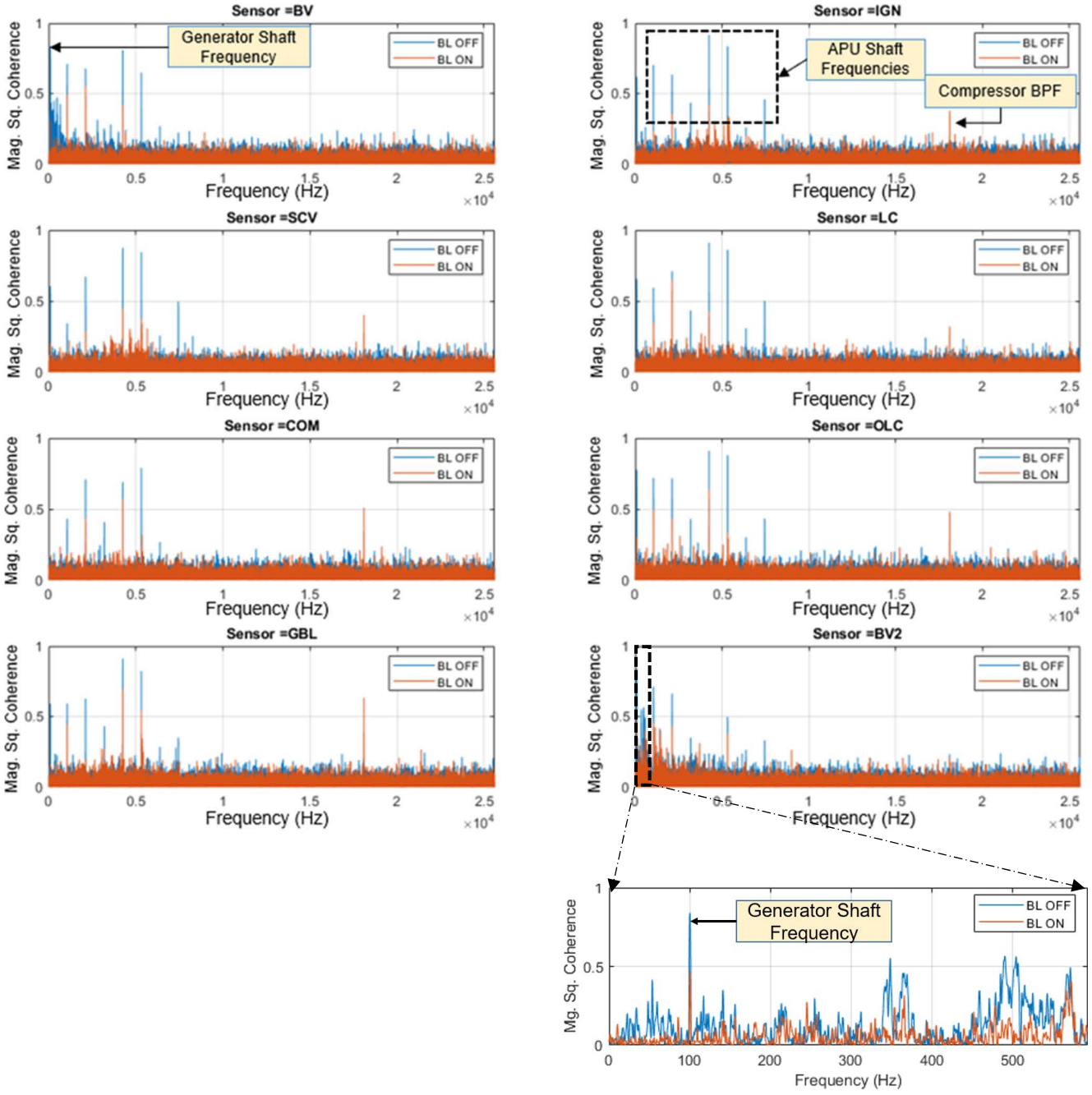

FIGURE 4. Coherence analysis between far-field and near-field acoustic data.

blade pass frequency (BPF) of 18kHz] are slightly coherent with the far-field microphone data, with the coherence levels reducing further under BL ON conditions. Furthermore, the low-frequency (combustion) noise has not been found to be coherent with any of the inside shroud sensors. BV and BV2 sensors show a certain level of coherence at low frequencies, being slightly distant to the APU as compared to the remaining sensors, but coherence levels are not sustained under BL ON conditions where APU noise due to vibrations becomes dominant (see the zoomed-in figure for sensor BV2).

Based on the analysis, it can be concluded that the near-field microphones close to the APU are overwhelmed by the noise generated by engine vibration and pneumatic flows inside the APU compartment and are therefore unable to sense the variations in the combustion noise taking place in the far-field of the APU. Moreover, the combustion noise from the far-field may also be getting attenuated while traversing through the aircraft structure and the APU shroud. The absence of the typical combustion spectra at any of the sensor locations (analysis not shown) further substantiates

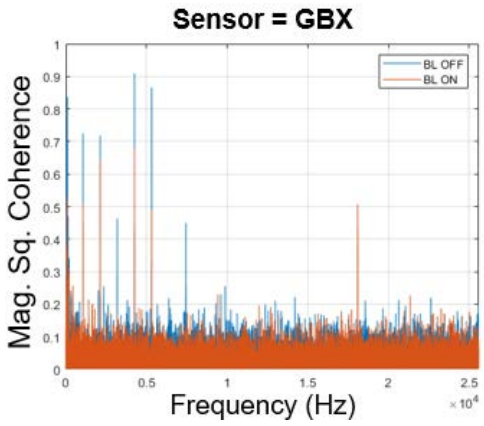

FIGURE 5. Coherence analysis between far-field acoustic and APU vibration data.

TABLE 1. Number of tones with coherence greater than 0.5.

	BL OFF	BL ON
BV	27	3
LC	82	14
IGN	19	11
SCV	22	12
COM	17	11
GBL	83	23
OLC	61	18
BV2	35	8

this outcome. The analysis has been expanded to include coherence of the far- field microphone data with the vibration sensor [GBX] (Fig. 5). The results are similar to the ones with the microphone data and show that the vibration sensor also cannot sense the combustion noise. This can be because of the design of the APU combustor and structure which restricts the induction of low-frequency acoustic waves into the structure to avoid acoustic fatigue. This suggests that combustion noise levels cannot be estimated by microphones and vibration sensors inside the APU compartment *{Finding # 1}*. On the other hand, the shaft frequencies are coherent with the far-field microphone data, thus making an external microphone suitable for monitoring the APU shaft faults *{Finding # 2}*.

B. TONAL ANALYSIS

In this section, a detailed analysis of the tonal frequencies acquired by the near-field microphones is presented. Initially, the outcomes of the coherence analysis between the microphone and a reference vibration sensor are discussed. The effect of sensor locations on coherence estimates is also presented. Secondly, an in-depth analysis of the frequency response of the acoustic data is performed. Lastly, the performance of Bicoherence analysis on acoustic data is presented, for which the Higher-Order Spectral Analysis Toolbox, developed for MATLAB [34], has been utilized.

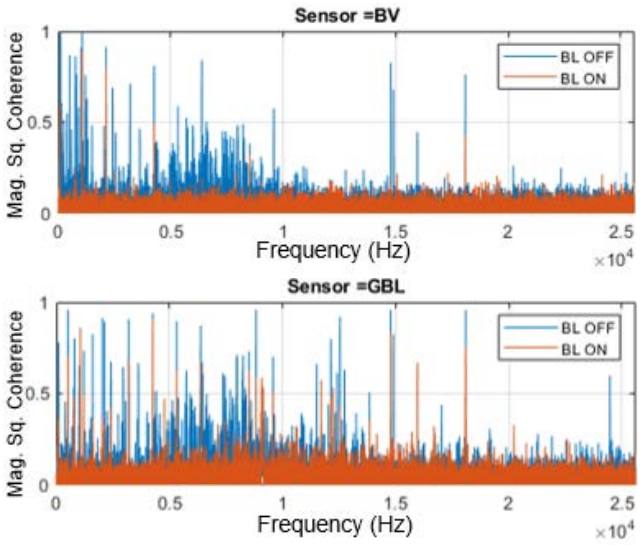

FIGURE 6. Coherence analysis between near-field acoustic sensors and vibration data.

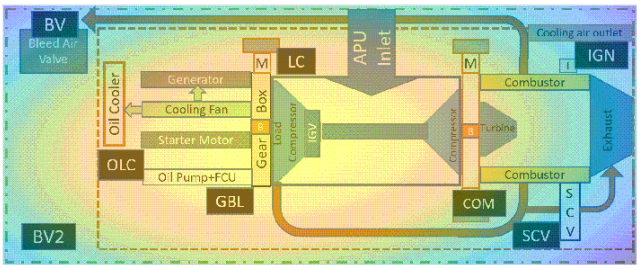

FIGURE 7. Variation in the number of coherent tones across APU.

1) COHERENCE ANALYSIS BETWEEN ACOUSTIC AND VIBRATION SENSORS

Coherence analysis has been performed between the vibration sensor installed on the APU gearbox and the near-field microphones under BL OFF and BL ON states (two of the results are shown in Fig. 6). Under the BL OFF state, a large number of tones display a certain level of coherence, however, under the BL ON case the tones are no longer coherent. Table 1 provides a summary of the number of tones that have coherence greater than 0.5 at various sensor locations. The drastic reduction in the number of coherent tones is visible across all the sensor locations under BL ON conditions, with the GBL microphone being able to retain 23 coherent tones due to its proximity to the source. On the contrary, the microphones farthest from the gearbox show a downward trend. Fig. 7 shows this information overlaid on the APU schematics using a surface plot, where the color represents the number of coherent tones (brighter color indicates a greater number of coherent tones and vice versa). It can be concluded that the region around the gearbox can be an appropriate choice to observe some of the tonal frequencies. However, as per

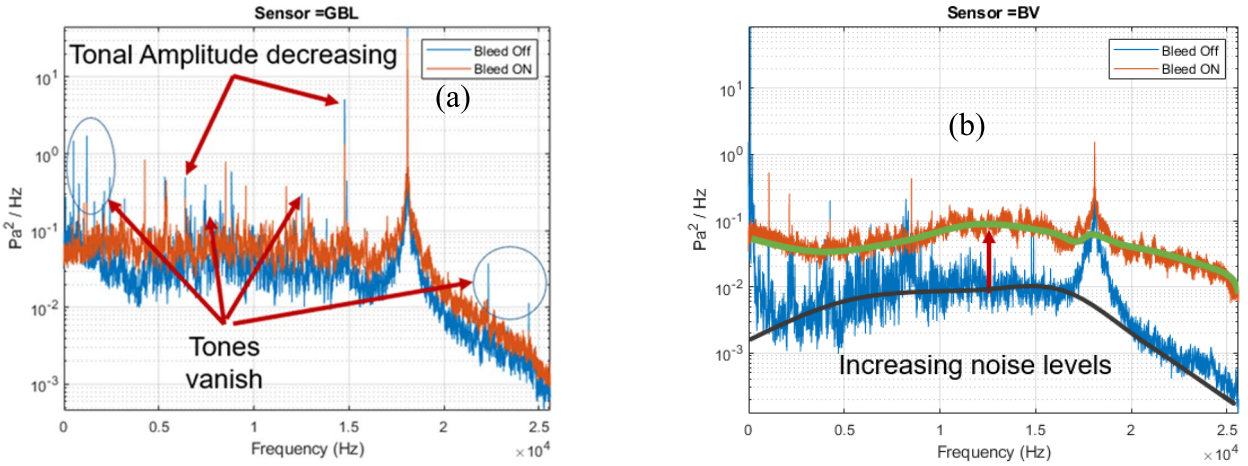

FIGURE 8. Power spectrum of acoustic data from microphones at location (a) GBL and (b) BV.

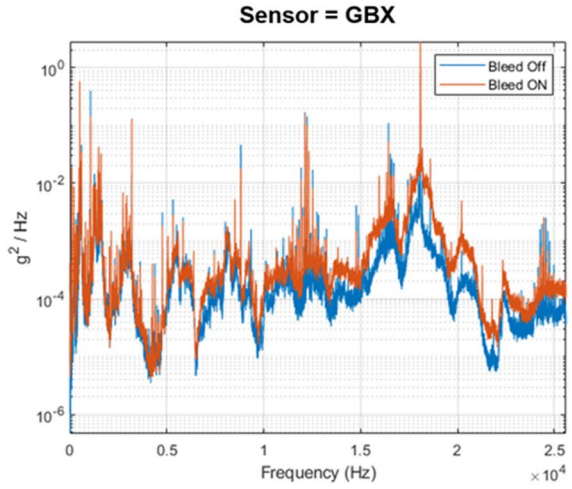

FIGURE 9. Power spectrum of gearbox vibration data.

the analysis (not shown), only the shaft frequencies are in a majority amongst the coherent tones while the remaining ones get hidden behind the background noise (especially under BL ON conditions) *{Finding # 3}*. Possible reasons for the deterioration in the coherence results under the BL ON state are explained in subsequent paragraphs.

Consider the power spectrum of the acoustic data from two of the sensor locations (GBL and BV) under BL OFF and BL ON states (Fig. 8). The clear distinction between the two states is visible from the figure in terms of reduction in the amplitudes / weakening of certain tones and the increase in the overall noise levels for BL ON states. These effects (some of which have been highlighted in the figure) are more pronounced at sensor location BV which is outside the shroud. This sensor is only able to retain four tones corresponding to shaft frequencies and the compressor blade-pass-frequency. All the other tones are overwhelmed by the background noise.

In order to identify the possible source of these effects, the frequency power spectrum of the vibration data corresponding to the same APU states is presented in Fig. 9. Firstly, it is evident that the vibration sensor is less affected by the change in the APU state as it only shows a very slight reduction in some tonal amplitudes. There is, however, some increase in the vibration levels for frequencies above 7 kHz, but the increase is still small enough not to completely conceal the tones. The vibration characteristics remain unaffected by the combustion noise (which is present at low frequencies) *{Finding # 4}*. After conducting this analysis, the disparity between the vibration and acoustic sensors (in terms of the degradation of tones amplitudes under BL ON conditions for acoustic sensors) can be explained to be because of the combined effect of the increase in the overall noise levels and decrease in tonal amplitudes. The increase in the overall noise floor can be because of the microphones being sensitive to the variations in the flow noise. For the reduction in tonal amplitudes, two phenomena have been identified which may be causing this effect: RPM fluctuations and the Doppler effect.

2) EFFECT OF RPM FLUCTUATIONS ON TONAL FREQUENCIES

In the absence of the raw RPM signal from the APU to determine the extent of RPM fluctuations, the power spectrum has been used to ascertain the extent of fluctuations. Fig. 10 shows the power spectrum of the vibration and acoustic data by dividing the data into one-second segments, which have been zoomed into the tone at 12.53kHz. The tone appears to be quite stable (not fluctuating its position in terms of frequency) under BL OFF conditions for both the vibration and acoustic data. Whereas the same tone is shifting back and forth under BL ON conditions for vibration data. This, in turn, distorts the tone in the acoustic data which is evident from the figure. The net effect is the reduction in the amplitude and increase in the spread of tones for both types of sensors.

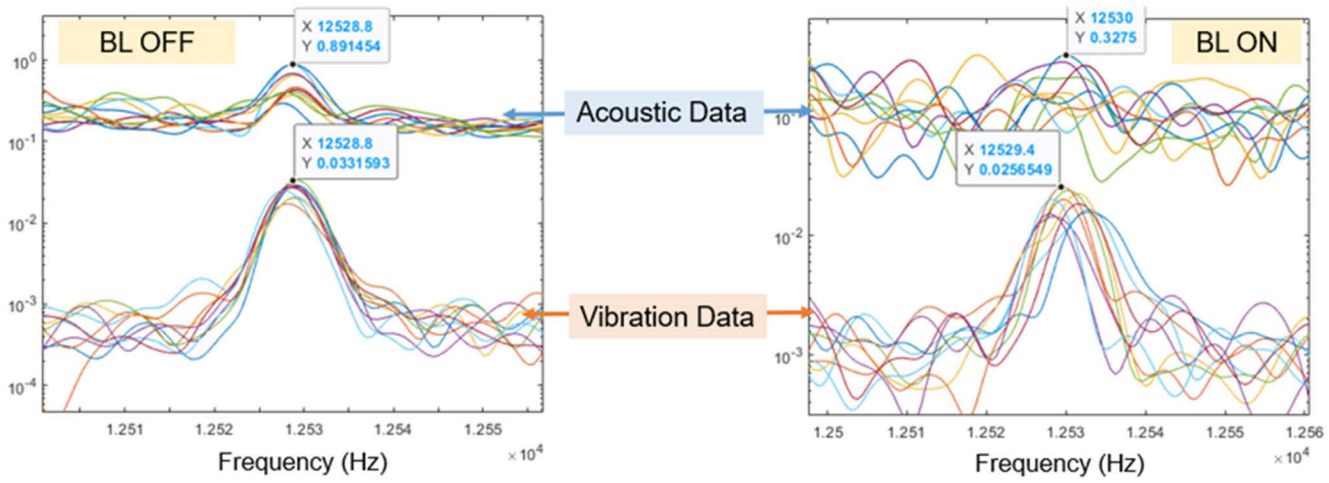

FIGURE 10. Power spectrum of the segmented versions of vibration and acoustic data.

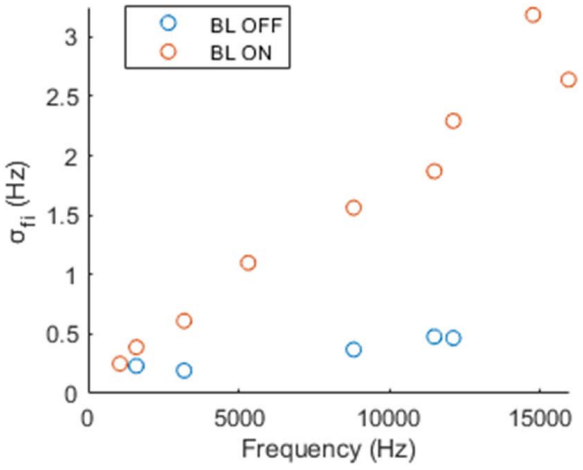

FIGURE 11. Deviation in tonal frequencies during BL OFF and BL ON states.

In order to quantify the degree of RPM fluctuations under BL OFF and BL ON conditions using experimentally acquired data, certain tones (for example 12.53 kHz) in the vibration data have been chosen for analysis. For each of the one-second data segments, the location of the tones (f_i) is noted using MATLAB's *'findpeaks'* function, and eventually, the deviation for each frequency (σ_{fi}) is computed. The process is carried out for both cases (five tones for BL OFF and nine tones for BL ON) and the results are presented in Fig. 11. There is a distinct difference between both states. Under low load conditions, the deviation in the frequencies is low (maximum σ_{fi} of 0.5Hz), whereas for high load conditions the deviations are high. Moreover, for high frequencies, the deviations are high as well, which confirms that the fluctuations are related to the variations in the RPM because the higher-order tones are affected more as compared to the ones with lower orders.

Consider a tonal frequency generated by a component that is rotating at a multiple of n_i with respect to the APU RPM, that is,

$$f_i = n_i RPM/60 \tag{6}$$

Conversely, the term n_i can be computed if the average RPM ($\overline{RPM}$) and average frequency ($\bar{f}_i$) are known:

$$n_i = 60\bar{f}_i/\overline{RPM} \tag{7}$$

If the RPM is fluctuating with σ_{RPM}, there will be equivalent fluctuation in the tonal frequencies (σ_{fi}) which is given by:

$$\sigma_{fi} = n_i \sigma_{RPM}/60 \tag{8}$$

Or,

$$\sigma_{RPM} = 60\,\sigma_{fi}/n_i \tag{9}$$

Combining 7 and 9 give,

$$\sigma_{RPM} = \sigma_{fi}\,\overline{RPM}/f_i \tag{10}$$

Since there are multiple tonal frequencies generated by the APU, σ_{RPM} computed from the individual tones (f_i) can be averaged to provide an accurate estimation of RPM fluctuations ($\bar{\sigma}_{RPM}$),

$$\bar{\sigma}_{RPM} = \frac{\overline{RPM}}{N}\sum_i \frac{\sigma_{fi}}{f_i} \tag{11}$$

where 'N' is the number of tones used for the analysis.

The analysis reveals that the average deviation in APU RPM ($\bar{\sigma}_{RPM}$) is 2.64 under lower load conditions which increases to 11.77 when the APU pneumatic system is activated. This, in turn, fluctuates the tones, and the variation is more for higher frequencies where n_i is high (equation 8). These fluctuating tones generated by the engine vibrations are translated into sound and the superposition of sinusoidal tones with varying amplitude, phase, and fluctuating frequencies takes place. The resultant effect is a decrease in acoustic

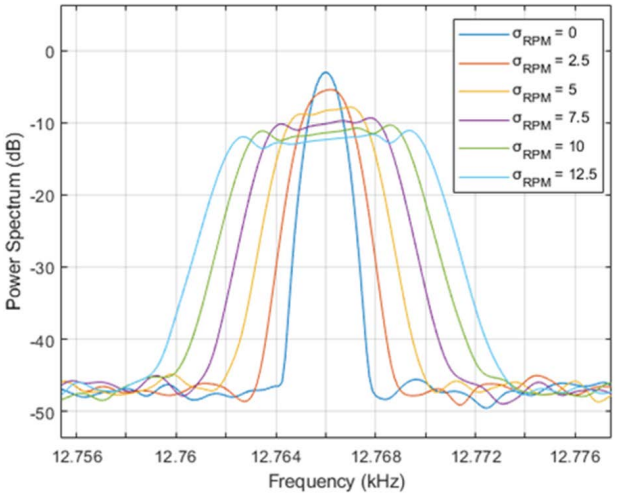

FIGURE 12. Power Spectrum of $S_{f12}(t)$ for different levels of RPM fluctuations.

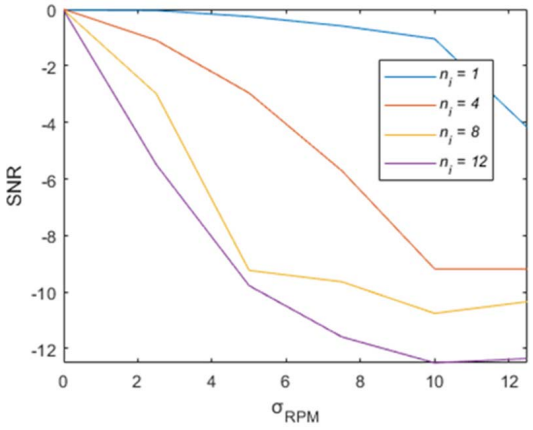

FIGURE 13. Effect of variation in RPM fluctuations on SNR of tones at various orders.

tonal amplitudes spread over a wider range of frequencies. The tones which display an opposite trend in their amplitudes are the resonating frequencies of the APU structure and are not affected by the change in RPM (see tone at 20kHz in Fig. 9).

To illustrate the effect of RPM fluctuations on the SNR of tones, the relationship between σ_{RPM}, n_i and SNR for a signal with a tone at f_i is studied using synthetically generated data. Consider a signal in which the tone f_i is varying due to RPM fluctuations:

$$S_{fi}(t) = sin(2\pi \int f_i(t)\,dt) + n(t) \tag{12}$$

where $n(t)$ is additive Gaussian noise, and f_i is related to RPM using relationship (6),

$$S_{fi}(t) = \sin(2\pi n_i/60 \int RPM(t)\,dt) + n(t) \tag{13}$$

$RPM(t)$ is simulated as a triangular wave with amplitude $A = \sqrt{3}\sigma_{RPM}$ [35] to generate the desired σ_{RPM}. The frequency of the triangular wave has been arbitrarily chosen to be 0.25Hz. MATLAB's '*sawtooth*' function has been used to generate the desired triangular wave [$tri(t)$], that is,

$$RPM(t) = \overline{RPM} + \sqrt{3}\sigma_{RPM}\,tri(t) \tag{14}$$

where $tri(t)$ is a triangular wave that spans in the range [−1,1]. By combining (13) and (14),

$$S_{fi}(t) = \sin\{2\pi n_i/60(\overline{RPM} + \sqrt{3}\sigma_{RPM} \int tri(t)\,dt)\} + n(t) \tag{15}$$

Using the above relationship, a set of signals [$S_{f1}(t)$, $S_{f4}(t)$, $S_{f8}(t)$ *and* $S_{f12}(t)$] have been derived corresponding to $n_i = [1, 4, 8$ *and* $12]$ for $0 \le \sigma_{RPM} \le 12.5$ with $\overline{RPM} = 63,830(1063.8Hz)$. For the required numerical integration, MATLAB's '*cumtrapz*' function has been used.

Fig. 12 shows the effect of varying σ_{RPM} on the tonal amplitude of the signal $S_{f12}(t)$ in the frequency domain. The amplitude can be seen to be decreasing as the RPM fluctuation increases. The tone also spreads in the frequency domain in the same way it has been noticed in the experimental data. Fig. 13 shows a summary of the analysis for all the considered tones. It can be seen that the SNR of the tones decreases with the increase in σ_{RPM}, and the effect is more pronounced for higher-order tones. This behavior will reciprocate in the acoustic data to an extent that the tones may totally disappear [see the vanishing tones highlighted in Fig. 8(a)].

3) DOPPLER EFFECT ON DATA COLLECTION

The tones produced by the APU undergo reflections by various surfaces inside the APU compartment and eventually reach the microphones. Some of these surfaces are under continuous oscillations, and the acoustic waves propagating inside the compartment are incident on those vibrating surfaces. Moreover, since the microphones are installed on wires / cables, they also experience a certain level of shaking. Under such circumstances, the acoustic waves encounter a Doppler effect due to the vibrations of surfaces / microphones with a multitude of frequencies. To study this phenomenon, an experiment has been set up that includes a tone-generating instrument, which is kept stationary, and a microphone installed on a shaker to generate vibrations (Fig. 14).

Acoustic data from the microphone is sampled at 11.025 kHz and a 1kHz tone is transmitted from the speaker. Five sets of data are acquired by varying the shaker vibration frequencies (0-40Hz with an interval of 10Hz). Fig. 15 shows the frequency power spectrum of the acquired acoustic data. Apart from the tones and harmonics corresponding to the selected vibration frequency (not shown in the figure), modulation of the transmitted 1kHz tone is taking place, which leads to sidebands corresponding to $1kHz \pm n\,f_{shaker}$, with the amplitude of the sidebands diminishing for higher values of n. For example, with $f_{shaker} = 30$Hz, the sidebands occur at around 1.03kHz and 0.97 kHz for $n = 1$. The slight reduction

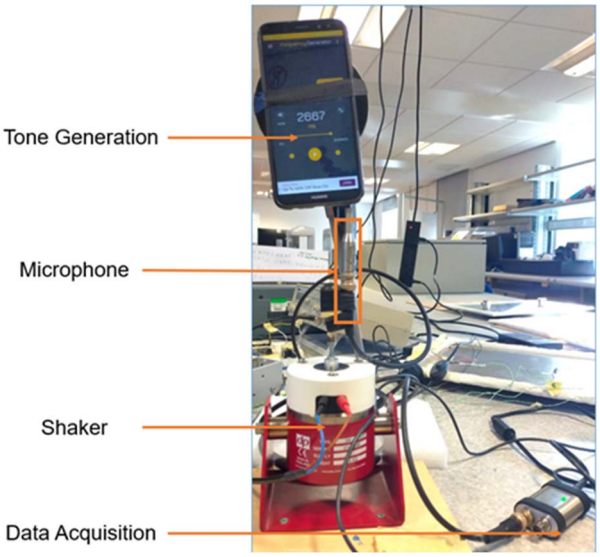

FIGURE 14. Experimental setup to study the effect of vibration on generated acoustic tones.

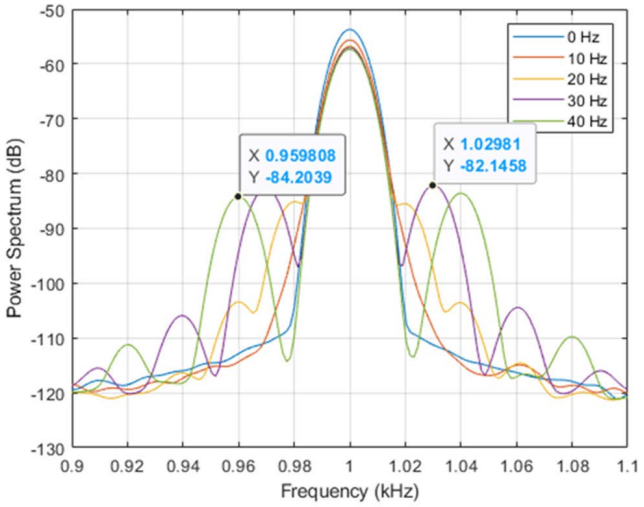

FIGURE 15. Power Spectrum of acquired acoustic data from the microphone undergoing vibrations.

in the 1kHz tonal amplitude is also visible when compared with the shaker in a stationary condition. These results are in agreement with previous work [36], where a slightly different experiment was set up and a very high frequency (225 kHz) was used.

The combined effect of RPM fluctuations and the Doppler effect is the superposition of multiple tones generated by the components and sidebands due to the acoustic reflections from vibrating surfaces. The sidebands can also interfere with the frequencies of interest and thus render them ineffective for condition monitoring purposes. Moreover, as the tones move back and forth, due to RPM fluctuations, their superposition may lead to a reduction in their amplitude due to phase mismatch during propagation inside the APU compartment. Furthermore, since the vibrations are taking place at multiple frequencies, a clear separation between the tone and the sidebands will not be present, and the tonal frequency will spread over a wider range. Under such circumstances, the appearance of any new tonal frequency or an increase in the amplitudes of the already existing frequencies (which has not been detected under healthy conditions using microphones) due to a faulty condition cannot be captured through the deployment of microphones in the APU compartment.

4) BICOHERENCE ANALYSIS

Vibration signals measured from a rotary machine can have many forms of amplitude and phase modulations which can indicate a large range of failure conditions [37], [38]. High-order spectral techniques (like Bicoherence) can detect such modulations which are otherwise not visible in the frequency spectrums. In this study, the possible utilization of Bicoherence analysis on near-field acoustic data is assessed. In the absence of detailed information about the system parameters, Bicoherence graphs of the vibration data have been considered as a reference, and the possibility of those graphs getting reciprocated in the acoustic data is ascertained. The parameters selected for Bicoherence analysis are similar to the ones for coherence (described in Section III.C), however, the FFT size is chosen to be 512 to reduce the computational requirements.

The Squared Bicoherence values for vibration data from sensor GBX during BL OFF and BL ON states are shown in Fig. 16. Phase coupling can be seen to be occurring between 100Hz and 12.1kHz. The Bicoherence at this pair of frequencies remains almost constant and has been found to exist at locations GEN and GBY (results not shown). The Bicoherence value for GBX decreases slightly (0.6 to 0.5) under the BL ON state, which is attributable to the increase in the overall vibration levels and decreasing tonal amplitudes (SNR decreasing). Treating the identified phase-coupled frequency pair as a reference, the same analysis is repeated for acoustic data [sensor = GBL] (Fig 17). The resultant graphs do not reproduce similar results regardless of the APU state. Moreover, any other phase-coupled frequency pairs do not surface across the whole spectrum, which renders Bicoherence analysis on highly noisy (acoustic) data completely ineffective to generate any useful information about the system *{Finding # 5}*.

To observe the effect of SNR on Bicoherence results, the process is repeated on synthetically generated data with known phase coupling and varying SNR. A phase-modulated signal is created with a sinusoidal carrier ($f_c = 1300Hz$) and sinusoidal signal ($f_m = 5100\ Hz$) with the sampling frequency of 51.2kHz using the following relationship:

$$S(t) = S_{pure}(t) + n(t) \tag{16}$$

where,

$$S_{pure}(t) = \sin(2\pi f_m t + \varphi_m) + \sin[2\pi f_c t + \sin(2\pi f_m t)] \tag{17}$$

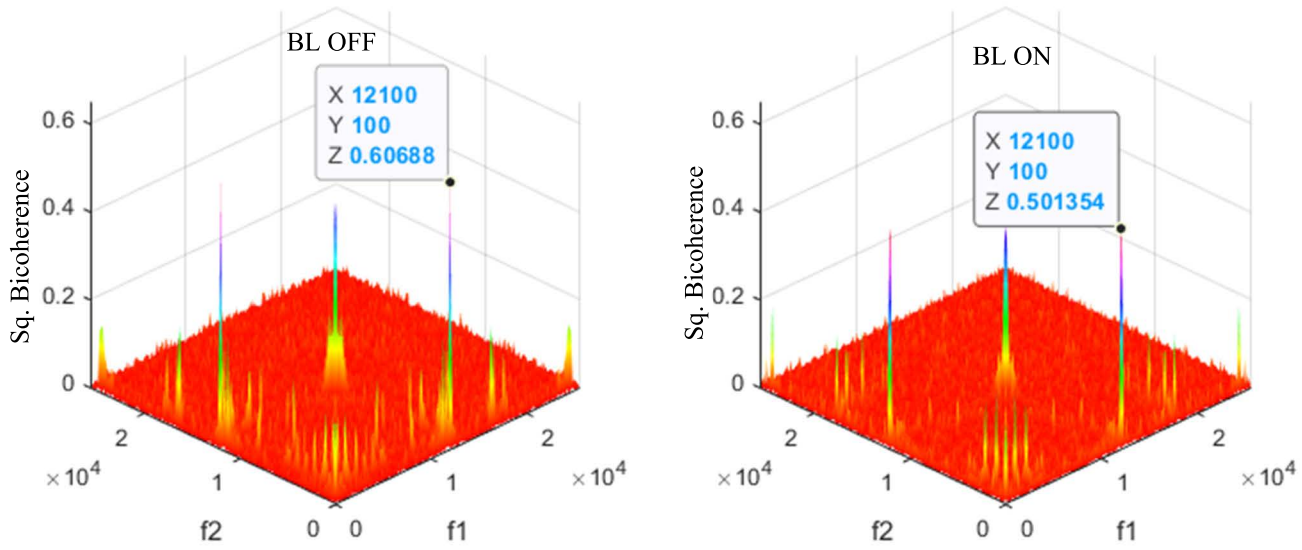

FIGURE 16. Bicoherence analysis of vibration data.

The noise power $[\sigma^2_{n(t)}]$ of the added normally distributed noise $[n(t)]$ is varied to produce three sets of signals with different SNRs [0dB, −15dB, and −20dB]. SNR is computed using the following relationship:

$$SNR = 10 \log \left(\sigma^2_{S_{pure}(t)} \Big/ \sigma^2_{n(t)} \right) \tag{18}$$

The results of Bicoherence estimates on the simulated signals are shown in Fig. 18. At 0dB SNR, the phase coupling between 1300Hz and 5100Hz is visible with a high value of Bicoherence. The estimated Bicoherence value reduces to 0.28 at SNR = −15dB and eventually diminishes to almost zero at SNR of −20dB. The results are similar to [39] where a different phase coupling model was used to report that Bicoherence fails to reliably detect phase coupling when SNR is less than −16 dB (or S/N = 0.158). As per their analysis [39, Fig. (3)], for a sq. bicoherence of 0.6 [computed for the vibration sensor – Fig. 16(a)], SNR of −4 dB (or S/N = 0.63) is required. Since no phase coupling is detected in the acoustic data, it implies that, during vibration to acoustic conversion, SNR reduces by at least 0.158 / 0.63 = 1/4 to produce a signal which has an SNR ≤ −16dB at which bicoherence does not produce useful results. The reduction in SNR can be because of the combined effect of the decrease in the tonal amplitudes and the increase in the noise floor for microphone data (the effects have been shown in Fig. 8).

C. BROADBAND NOISE ANALYSIS

This section presents the results acquired based on the analysis described in section III.E. Initially, the results for coefficients of overlap for calculated features are presented and discussed. This is followed by a detailed discussion of the computed correlation coefficients between vibroacoustic data and the considered APU parameters. Lastly, the possibility of external sources affecting the near-field acoustics is presented.

1) COEFFICIENTS OF OVERLAP

A significant amount of near-field acoustic, vibration and FADEC data has been acquired for this study. Several categories of features (mentioned in section III.E.1) have been computed in order to proceed with the desired analysis. The acquired dataset consists of 13,879 data points (corresponding to one-second data segments), out of which 6,265, 4,098, and 3,516 correspond to BL OFF, BL ON NL, and BL ON NL conditions, respectively. For any data point, there are 8 × 5 × 20 features from eight microphones and 3 × 5 × 20 from vibration sensors, where there are 5 feature categories and the approximate number of features in each category is 20. For computing the coefficients of overlap ($\Delta^{BL\ ON}_{BL\ OFF}$, $\Delta^{BL\ ON\ LD}_{BL\ ON\ NL}$), the kernel density for each of the features is computed separately for BL OFF, BL ON, BL ON NL, and BL ON LD states, and then expressions (1) and (2) are employed.

Fig. 19 illustrates the process of computing $\Delta^{BL\ ON}_{BL\ OFF}$ for a time-domain feature (RMS value) for each of the acoustic and vibration sensors. The figure shows that the RMS value is a good feature to separate between BL OFF and BL ON conditions for acoustic sensors BV and BV2, both of which are outside the APU shroud. OLC is the only sensor inside the shroud which exhibits a similar behavior and provides a lower overlap (0.13). Apart from these sensors, the RMS values have overlapping distributions for the remaining sensors, including the vibration sensors. Fig. 20 shows the same procedure repeated for $\Delta^{BL\ ON\ LD}_{BL\ ON\ NL}$ but with a different feature (the fifth feature of MFCC). It is evident from the figure that the two APU states (BL ON NL and BL ON LD) cannot be distinguished using this feature. However, the microphones installed near the igniter and the surge control

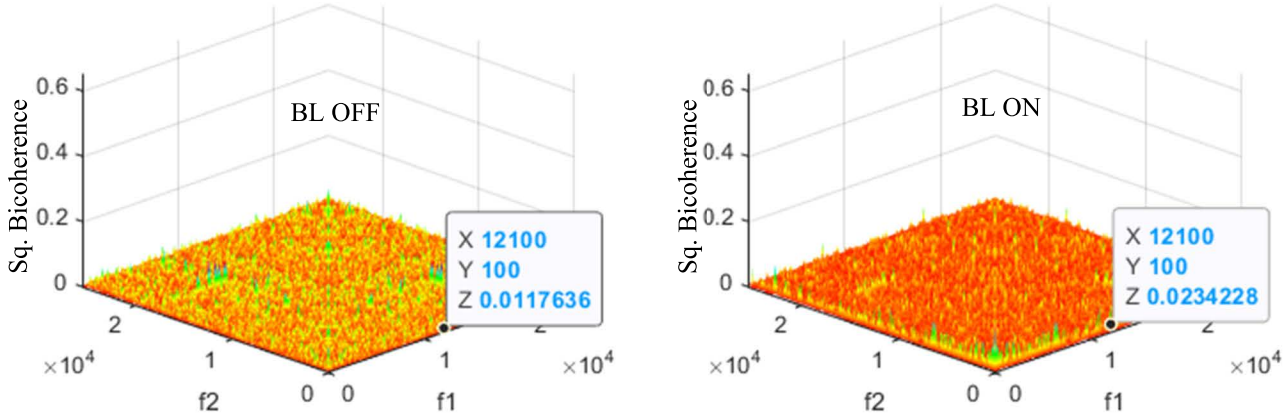

FIGURE 17. Bicoherence analysis of acoustic data.

valve demonstrate better performance. These two locations are closest to the bleed duct and therefore have a better chance of acquiring any change in acoustic characteristics due to flow variations.

Figures 19 and 20 have considered each microphone and vibration sensor separately to illustrate the employed scheme for computing the coefficients of overlap, each for a single feature. However, in order to provide a summarized version of the results, the two coefficients ($\Delta_{BL\ OFF}^{BL\ ON}$, $\Delta_{BL\ ON\ NL}^{BL\ ON\ LD}$) have been accumulated (refer to expression (3)) while keeping segregation between feature categories (Section III.E.1) and sensor type. Fig. 21 shows the distributions of the overlap coefficients for each of the five categories of features, separately for acoustic and vibration sensors. Considering $\Delta_{BL\ OFF}^{BL\ ON}$ first, the results show that a clear separation between BL OFF and BL ON states can be made (i.e., several features demonstrate zero values of overlap coefficient) regardless of the sensor and the category of feature extraction technique used [Fig. 21(a)] *{Finding # 6}*. The acoustic data, however, offers a larger number of features (32%) with zero overlaps as compared to the vibration data where only 10% of the features can reliably separate the two states using a given feature category. Furthermore, the 'BandPowers' have the highest number of lower $\Delta_{BL\ OFF}^{BL\ ON}$ values for both sensor types and may prove to be a better choice for developing classification models if all the sensors are concurrently considered. The ability of the vibroacoustic sensors to be able to segregate between the BL OFF and BL ON states stems from the fact that numerous changes take place when the APU's pneumatic system is activated, which can be easily picked up by these sensors. In BL ON states (BL ON NL / NL ON LD), IGVs open increasing the mass flow through the Load Compressor, Surge Valve and Bleed Valve. This increases the torque required by the load compressor. To keep the APU RPM constant under such conditions, the fuel flow to the combustor increases thus increasing the combustion noise. The combined effect is the increase in vibrations and noise across the whole APU, which can be picked up by vibroacoustic sensors with appropriate feature extraction techniques.

The situation is considerably different when segregating between BL ON NL and BL ON LD states, which is evident from Fig. 21 (b). There is a distinct difference between the response of the acoustic and vibration sensors, as the latter does not show promising results. The values of $\Delta_{BL\ ON\ NL}^{BL\ ON\ LD}$ for the vibration sensors are high ($\Delta > 0.3$) regardless of the technique used, while for the acoustic data there are some features for which the values of coefficients are close to zero which is desirable *{Finding # 7}*. This behavior can be attributed to the fact that, between the two APU states, only the mass flow through the surge valve and the bleed valve varies, while everything else remains the same. The flow variations lead to changes in acoustic characteristics around the bleed duct, which may not get induced as vibrations and picked up by the vibration sensors. Amongst the feature categories, certain features from MFCC and BandPower exhibit better performance on acoustic data, where the former slightly outperforms the latter using acoustic data *{Finding # 8}*.

2) CORRELATION COEFFICIENTS

In this section, the distribution of the correlation coefficients accumulated using: different categories of features; microphone and vibration data; and various APU parameters, is presented. The distributions depict the number of features that are correlated / uncorrelated with a specific APU parameter. The desired response of a distribution is to have a minimum number of features exhibiting zero correlations, while the maximum is highly correlated (i.e. $|\rho| \approx 1$). Such a distribution will imply that the majority of the features in that category change linearly with an APU parameter, or in other words, most of the features are directly affected by only that parameter and uninfluenced by any other variation taking place in the APU.

The amount of data utilized for this analysis consists of: 13,897 data points (corresponding to all APU states) to compute ρ_{TOil} and ρ_{mLC}, 7,614 data points (corresponding to BL ON states) to compute ρ_{IGV}, and 3,516 data points (corresponding to all BL ON LD states) to compute ρ_{mBleed}.

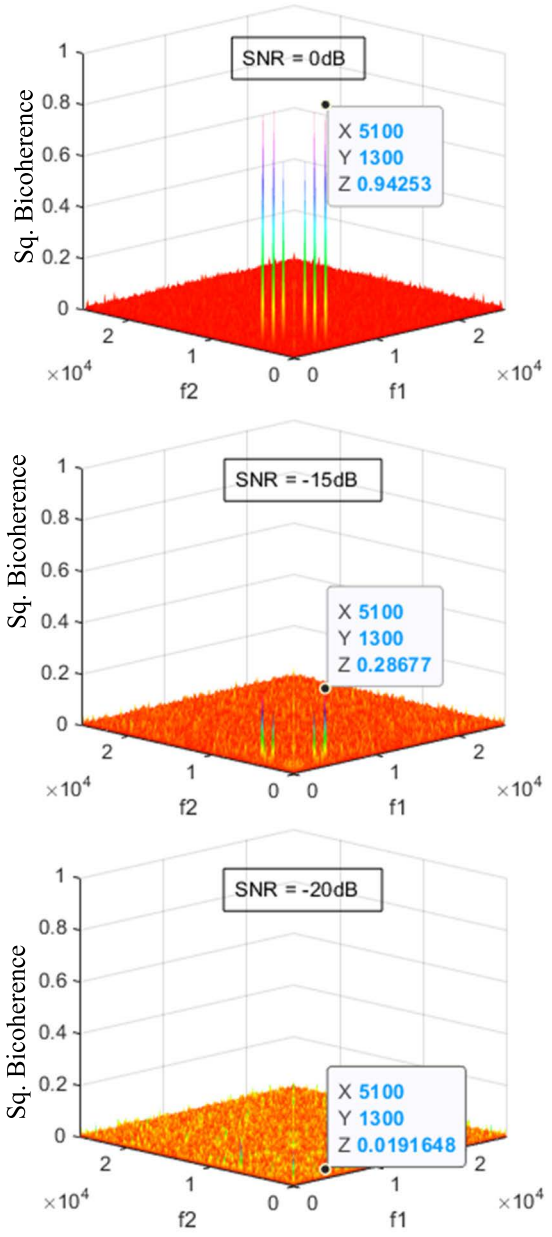

FIGURE 18. Result of bicoherence analysis on simulated data.

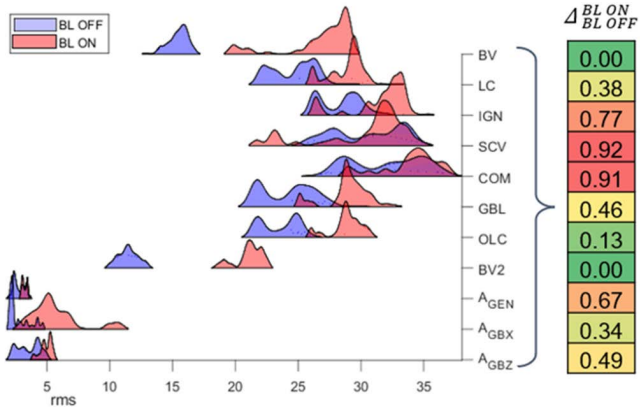

FIGURE 19. Results of $\Delta^{\text{BL ON}}_{\text{BL OFF}}$ for RMS feature (Time domain feature category) for all the sensors.

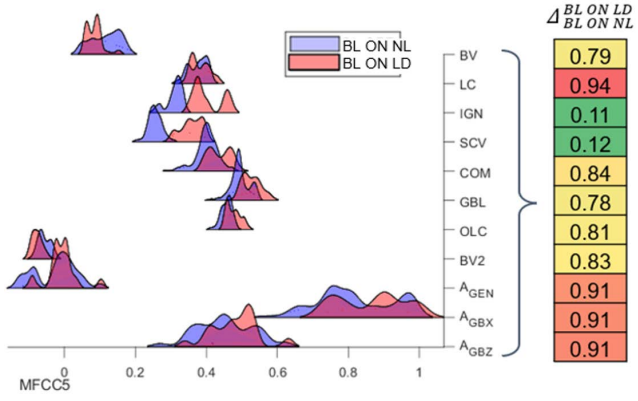

FIGURE 20. Result of $\Delta^{\text{BL ON}}_{\text{BL OFF}}$ for the fifth feature (MFCC feature category) for all the sensors.

The result of the complete analysis is presented in Fig. 22 which gives the complete picture of the distributions of the computed correlation coefficients while segregating between acoustic and vibration data for all the five categories of feature extraction techniques (refer to expression (5)).

Considering T_{oil} first [Fig. 22 (a)], the superiority of vibration sensors over acoustic sensors can be clearly observed. The values of $[\rho_{TOil}]_{vibration}$ range between -1 and 0.9, whereas for $[\rho_{TOil}]_{acoustic}$ the values are between -0.9 and 0.8. Moreover, the ratio of features exhibiting higher correlations is also high for the vibration sensors. This makes the vibration sensors a better choice utilizing them to estimate the oil temperature *{Finding # 9}*. MFFC features using vibration sensors have been identified as the best feature extraction technique for this purpose. The situation is different for the other three APU Parameters ($\dot{m}_{LC}$, IGV angles, and $\dot{m}_{bleed}$), with the acoustic sensors showing better correlations as compared to their counterpart. The values of $[\rho_{mLC}]_{acoustic}$ have been found to be nearly ± 1 using any of the feature extraction techniques [Fig. 22 (b)] which makes the acoustic sensors a suitable candidate for developing a regression model for monitoring the performance of the load compressor *{Finding # 10}*.

A greater deviation between the two types of sensors can be observed when computing correlations with IGV angles [Fig. 22 (c)]. With the acoustic sensors, $|\rho_{IGV}|$ values can be as high as 0.85 with certain MFCC features, while they are below 0.75 with the vibration sensors regardless of the feature extraction technique used. This may be attributed to the vibration sensor being sensitive to localized variations in the vibrations and therefore not being able to capture a wide range of variations taking place due to the change in APU operating characteristics. Within the acoustic sensors, it can be observed that the Time Domain and BandPower features are not the most desirable set of inputs for regression

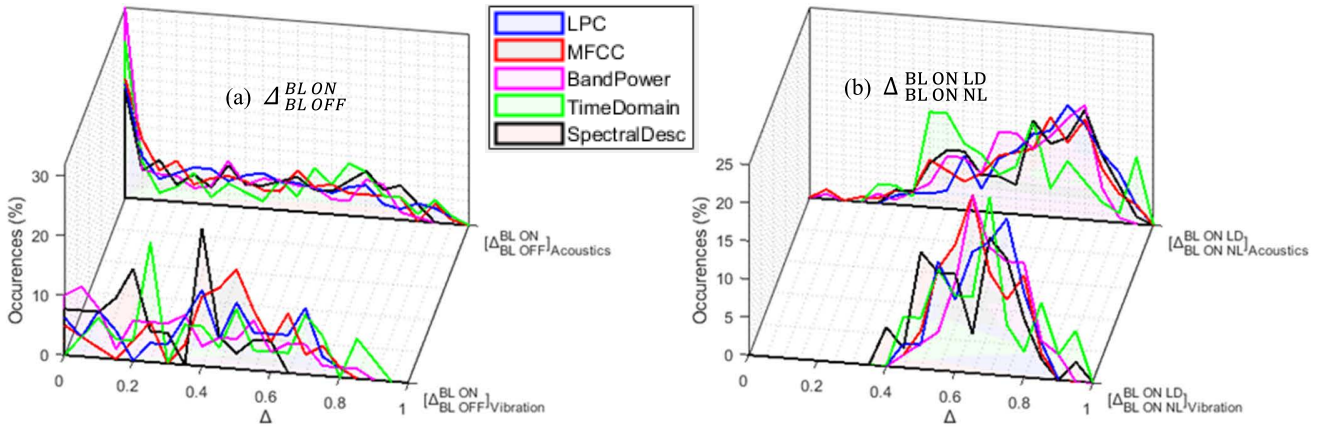

FIGURE 21. Distributions of coefficients of overlap for different categories of acoustic and vibration features.

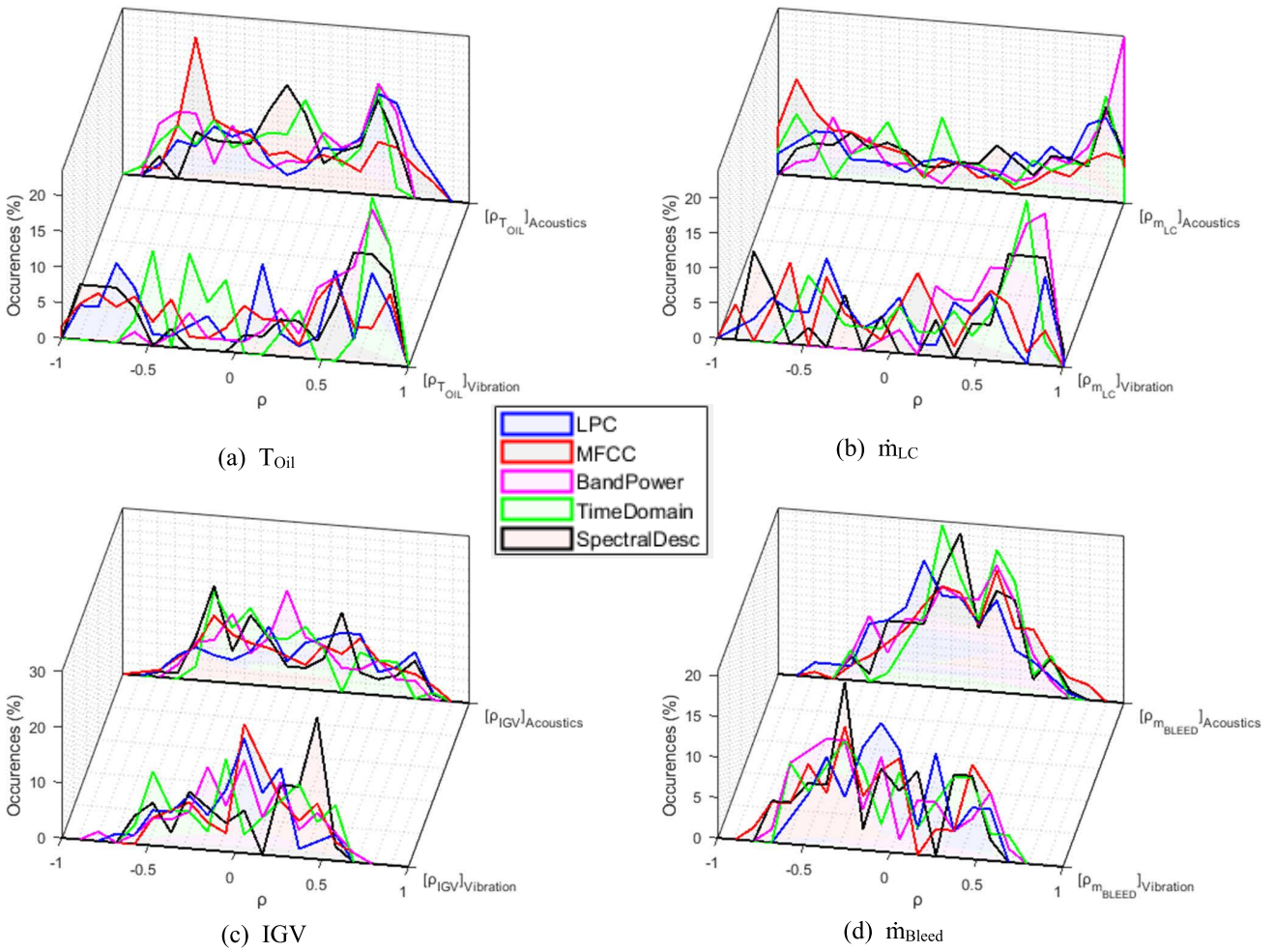

FIGURE 22. Distributions of correlation coefficients for APU parameters and different categories of features.

since most of the features are uncorrelated. Lastly, acoustic sensors have also been found to be better in terms of higher values of correlations between the derived features and mass flow through the bleed valve $[\rho_{mBleed}]_{acoustic}$ [see Fig. 22(d)]. Either of the LPC and MFCC features can be used to provide correlations $|\rho_{mBleed}| > 0.8$, making them suitable for developing a regression model to translate the raw acoustic data into meaningful information about the mass flow through the bleed valve *{Finding # 11}*.

3) EFFECT OF EXTERNAL NOISE SOURCES ON NEAR-FIELD ACOUSTICS

Having successfully demonstrated that the near-field acoustic features exhibit good correlations with APU operating states

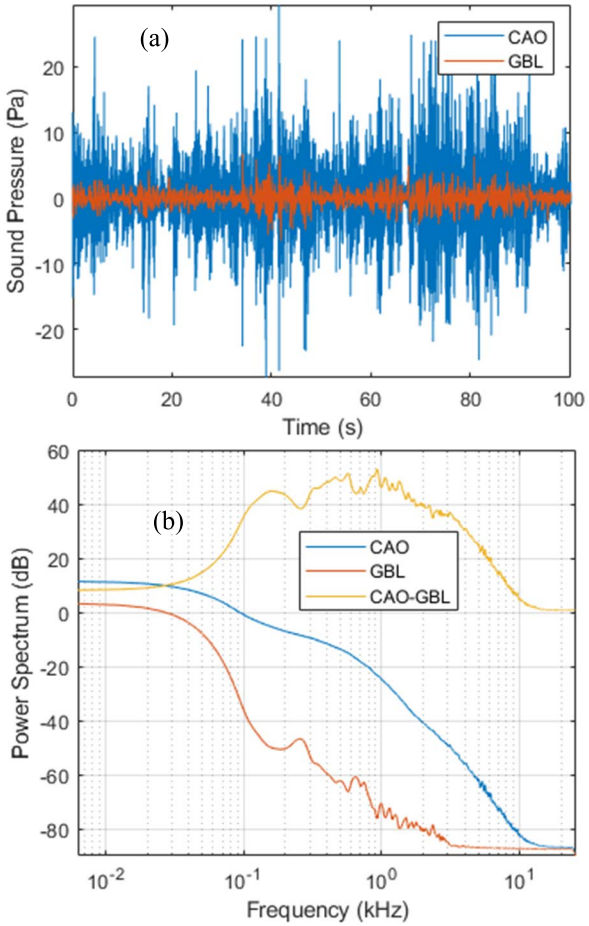

FIGURE 23. Analysis of external and internal microphone data (a) Time domain signal (b) Frequency Spectrum.

and performance parameters, this substantiates their potential to be implemented for APU condition monitoring purposes. In order to further strengthen their potential, the quantification of the effect of external noise sources on near-field acoustics needs to be addressed. To do this, the acoustics data corresponding to two microphones has been analyzed: one outside the APU compartment, mounted on the aircraft fuselage, labeled as Cooling Air Outlet (CAO), and the other one mounted inside of the APU shroud (GBL). Fig. 23 shows the time domain signal and power spectrum for both microphones when the APU is not in operation. From the time domain signal (Fig. 23(a)), it can be established that the (CAO) is more prone to external noise relative to the GBL. After listening to the audio files, the wind has been identified to be the major noise source for CAO, whereas for GBL it is mostly silent with faint sound due to the chirping of birds at around 40-50 seconds.

To further elaborate on the results, the frequency spectrum of acoustics data at CAO and GBL and their difference has been analyzed, shown in Fig. 23(b). Considering CAO first, it can be established that the external noise is present till 10kHz with the noise dominating between 0-100Hz region, after which the noise levels gradually decrease in the 100-10kHz range. Such noise, while traversing through the aircraft's metallic structure, experiences a frequency-dependent reduction in the noise levels that can be observed at sensor location GBL. For frequencies below 70Hz, the noise is attenuated by 10dB $-$20dB, and for frequencies above 100Hz, there is an average of 40dB reduction in the noise, which can reach a value of 53dB at 1kHz. As there is no background noise present for frequencies above 3kHz, the attenuation levels cannot be ascertained from this analysis. As reported in the literature, the sound attenuation increases for higher frequencies [40], therefore the acquired average attenuation level of 40dB can be extended for frequencies above 3kHz.

The aircraft's metallic structure and the APU shroud are responsible for attenuating the sound originating from external sources. As per the design, the APU is covered by the shroud for decreasing the noise produced by the APU as well as for containing flames in case of fire. This noise is further reduced by the aircraft structure which is holding the APU, elevators, and rudder. Such a reduction is favorable for the acoustic data captured inside the APU during operation since it will attenuate the external noise.

V. SUMMARY AND CONCLUSION

A comprehensive evaluation of the APU near-field acoustic data has been conducted to determine its potential for online condition monitoring purposes. To support this study, experimental data has been acquired from an in-situ aircraft APU under various load conditions, to generate an elaborate set of near-field and far-field acoustic, vibration, and APU state data. The acquired data is then processed to support the underlying scientific understating associated with the APU state and performance parameters, as well as its potential utility for online condition monitoring. The major results of this research work, collected from the *{Findings}* in the text, can be summarised as:

(a) Microphones (and vibration sensors) installed inside the APU compartment are not useful for capturing the combustion process (or combustion noise) *{Findings # 1 and 4}*. The noise generated from the APU vibration and the pneumatic system flows is dominant, which swamps the combustion noise propagation, either through the APU structure or from the APU exhaust.

(b) Microphones external to the APU compartment can monitor APU shaft frequencies for potential faults *{Finding # 2}*.

(c) The near-field microphones only capture part of the tonal frequencies generated by the shaft, bearing, and gearbox under low-load operating conditions. Under the high load operating conditions, the capability of the near-field microphones is further limited and has been demonstrated to predominantly capture tones corresponding to the frequency of the shaft *{Finding # 3}*. The possible reasons for the limited ability of the microphone for capturing the tones can stem from RPM fluctuations, the Doppler effect, and the rise in overall

noise levels due to the pneumatic flows through the load compressor, bleed duct, bleed valve, and the surge control valve.

(d) Bicoherence analysis is found to perform well on vibration data for condition monitoring. However, it fails to respond in the same manner for the acoustic data regardless of the APU operating state due to low SNR *{Finding # 5}*.

(e) Vibration and acoustic sensors are equally good in segregating between the two primary states of APU operation (BL OFF and BL ON) using any of the feature extraction techniques *{Finding # 6}*. However, the vibration sensors are unable to capture the variations taking place when the APU starts delivering flow through the Bleed Valve, which otherwise can be done with acoustic sensors using MFCC features *{Findings # 7 and 8}*.

(f) The acoustic data outperforms vibration data by demonstrating a high correlation with most of the APU performance parameters *{Findings # 9, 10, and 11}*.

The results acquired suggest that microphones have limited capability (as compared to the vibration sensors) to capture the tonal frequencies to enable condition monitoring of APU components (shaft, bearing, gears). However, the microphones prove to be an appropriate sensor for estimating the APU operating states and performance parameters to facilitate condition monitoring of lubrication oil cooling system and pneumatic system components (IGVs, SCV, and BV).

DATA AVAILABILITY

Data is restricted due to agreement with commercial partner.

REFERENCES

[1] U. Ahmed, F. Ali, and I. Jennions, "A review of aircraft auxiliary power unit faults, diagnostics and acoustic measurements," *Prog. Aerosp. Sci.*, vol. 124, Jul. 2021, Art. no. 100721, doi: 10.1016/j.paerosci.2021.100721.

[2] U. Ahmed, F. Ali, and I. K. Jennions, "Development of a far-field noise estimation model for an aircraft auxiliary power unit," *IEEE Access*, vol. 9, pp. 127703–127719, 2021, doi: 10.1109/ACCESS.2021.3112390.

[3] B. N. Shivashankara, "Gas turbine core noise source isolation by internal-to-far-field correlations," *J. Aircr.*, vol. 15, no. 9, pp. 597–600, Sep. 1978, doi: 10.2514/3.58412.

[4] J. Xu, C. Tam, and S. Parrish, "On indirect combustion noise," in *Proc. 50th AIAA Aerosp. Sci. Meeting Including New Horizons Forum Aerosp. Exposit.*, Jan. 2012, pp. 1–16, doi: 10.2514/6.2012-543.

[5] M. Pott-Pollenske, W. Dobrzynski, H. Buchholz, and D. Almoneit, "Characteristics of noise from aircraft ground operations," in *Proc. 28th AIAA Aeroacoustics Conf.*, May 2007, pp. 1–15, doi: 10.2514/6.2007-3560.

[6] R. L. Tubbs, "Case studies noise exposure to airline ramp employees," *Appl. Occupational Environ. Hygiene*, vol. 15, no. 9, pp. 657–663, Jan. 2010.

[7] K. Knobloch, A. Fischer, F. Bake, L. Enghardt, and S. Busse-Gerstengarbe, "Full-scale tests on APU noise reduction," in *Proc. ASME Turbo Expo.*, 2014, Art. no. V02AT41A011, doi: 10.1115/GT2014-26803.

[8] W. Jung, J. Bae, and Y.-H. Park, "Acoustic signal based non-contact ball bearing fault diagnosis using adaptive wavelet denoising," 2021, *arXiv:2110.03348*.

[9] S. V. V. S. N. Pichika, R. Yadav, S. Geetha Rajasekharan, H. M. Praveen, and V. Inturi, "Optimal sensor placement for identifying multi-component failures in a wind turbine gearbox using integrated condition monitoring scheme," *Appl. Acoust.*, vol. 187, Feb. 2022, Art. no. 108505, doi: 10.1016/j.apacoust.2021.108505.

[10] M. A. Khan, M. A. Shahid, S. A. Ahmed, S. Z. Khan, K. A. Khan, S. A. Ali, and M. Tariq, "Gear misalignment diagnosis using statistical features of vibration and airborne sound spectrums," *Measurement*, vol. 145, pp. 419–435, Oct. 2019, doi: 10.1016/j.measurement.2019.05.088.

[11] R. Giri, S. V. Tenneti, F. Cheng, and K. Helwani, "Unsupervised anomalous sound detection using self-supervised classification and group masked autoencoder for density estimation," Challenge on Detection and Classification of Acoustic Scenes and Events DCASE Challenge, DCASE2020, Tokyo, Japan, Tech. Rep. Task 2, 2020.

[12] R. K. Mobley, "Signature analysis," in *Vibration. Fundamentals*, Amsterdam, The Netherlands: Elsevier, 1999, pp. 181–188, doi: 10.1016/B978-075067150-7/50053-7.

[13] P. Raharjo, S. Abdussalam, F. Gu, and A. D. Ball, "Vibro-acoustic characteristic of a self aligning spherical journal bearing due to eccentric bore fault," in *Proc. 9th Int. Conf. Condition Monit. Machinery Failure Prevention Technol.*, 2012, pp. 124–140.

[14] T. Vaimann, J. Sobra, A. Belahcen, A. Rassõlkin, M. Rolak, and A. Kallaste, "Induction machine fault detection using smartphone recorded audible noise," *IET Sci., Meas. Technol.*, vol. 12, no. 4, pp. 554–560, Jul. 2018, doi: 10.1049/iet-smt.2017.0104.

[15] M. Holguín-Londoño, O. Cardona-Morales, E. F. Sierra-Alonso, J. D. Mejia-Henao, Á. Orozco-Gutiérrez, and G. Castellanos-Dominguez, "Machine fault detection based on filter bank similarity features using acoustic and vibration analysis," *Math. Problems Eng.*, vol. 2016, pp. 1–14, Dec. 2016, doi: 10.1155/2016/7906834.

[16] K. Shibata, A. Takahashi, and T. Shirai, "Fault diagnosis of rotating machinery through visualisation of sound signals," *Mech. Syst. Signal Process.*, vol. 14, no. 2, pp. 229–241, Mar. 2000, doi: 10.1006/mssp.1999.1255.

[17] C. Skliros, F. Ali, and I. Jennions, "Fault simulations and diagnostics for a boeing 747 auxiliary power unit," *Exp. Syst. Appl.*, vol. 184, Dec. 2021, Art. no. 115504, doi: 10.1016/j.eswa.2021.115504.

[18] H. Gupta and D. Gupta, "LPC and LPCC method of feature extraction in speech recognition system," in *Proc. 6th Int. Conf. Cloud Syst. Big Data Eng. (Confluence)*, Jan. 2016, pp. 498–502, doi: 10.1109/CONFLUENCE.2016.7508171.

[19] O. Eltiraifi, E. Elbasheer, and M. Nawari, "A comparative study of MFCC and LPCC features for speech activity detection using deep belief network," in *Proc. Int. Conf. Comput., Control, Electr., Electron. Eng. (ICCCEEE)*, Aug. 2018, pp. 6–10, doi: 10.1109/ICCCEEE.2018.8515821.

[20] O. Chia Ai, M. Hariharan, S. Yaacob, and L. Sin Chee, "Classification of speech dysfluencies with MFCC and LPCC features," *Exp. Syst. Appl.*, vol. 39, no. 2, pp. 2157–2165, Feb. 2012, doi: 10.1016/j.eswa.2011.07.065.

[21] M. Rana and S. Miglani, "Performance analysis of MFCC and LPCC techniques in automatic speech recognition," *Int. J. Eng. Res. Technol.*, vol. 3, no. 9, pp. 7727–7732, 2014.

[22] S. Oue, R. Marxer, and F. Rudzicz, "Automatic dysfluency detection in dysarthric speech using deep belief networks," in *Proc. 6th Workshop Speech Lang. Process. Assistive Technol.*, 2015, pp. 60–64, doi: 10.18653/v1/w15-5111.

[23] U. Bhattacharjee, "A comparative study of LPCC and MFCC features for the recognition of assamese phonemes," *Int. J. Eng. Res. Technol.*, vol. 2, no. 1, pp. 1–6, 2013.

[24] E. Raimy and C. E. Cairns, *The Segment in Phonetics and Phonology*. Hoboken, NJ, USA: Wiley, 2014, pp. 1–345, doi: 10.1002/9781118555491.

[25] Y. Petetin, C. Laroche, and A. Mayoue, "Deep neural networks for audio scene recognition," in *Proc. 23rd Eur. Signal Process. Conf. (EUSIPCO)*, Aug. 2015, pp. 125–129.

[26] B. Lehner, G. Widmer, and R. Sonnleitner, "On the reduction of false positives in singing voice detection," in *Proc. IEEE Int. Conf. Acoust., Speech Signal Process. (ICASSP)*, May 2014, pp. 7480–7484, doi: 10.1109/ICASSP.2014.6855054.

[27] S. Zhang, Y. Guo, and Q. Zhang, "Robust voice activity detection feature design based on spectral kurtosis," in *Proc. ETCS*, 2009, pp. 269–272, doi: 10.1109/ETCS.2009.587.

[28] B. Schuster and L. Lieber, "Narrowband model for gas turbine engine combustion noise prediction," in *Proc. 12th AIAA/CEAS Aeroacoustics Conf. 27th AIAA Aeroacoustics Conf.*, Cambridge, MA, USA, May 2006, pp. 1–13, doi: 10.2514/6.2006-2677.

[29] *Gas Turbine Jet Exhaust Prediction*, document ARP876F, SAE, 2013.

[30] J. W. Rawls and J. C. Yeager, "High speed research noise prediction code (HSRNOISE) user's and theoretical manual," NASA, Richmond, VA, USA, Tech. Rep. Nasa/Cr-2004-213014, Nov. 2004.
[31] G. R. Ibrahim and A. Albarbar, "Gearbox fault features extraction using vibration measurements and novel adaptive filtering scheme," *Adv. Acoust. Vibrat.*, vol. 2012, pp. 1–7, Jul. 2012, doi: 10.1155/2012/283535.
[32] L. T. Ikelle and L. Amundsen, *Introduction to Petroleum Seismology*. Houston, TX, USA: Society of Exploration Geophysicists, 2018, doi: 10.1190/1.9781560803447.ch6.
[33] O. M. Eidous and S. A. D. A. AL-Talafha, "Kernel method for overlapping coefficients estimation," *Commun. Statist. Simul. Comput.*, vol. 51, no. 9, pp. 5139–5156, Sep. 2022, doi: 10.1080/03610918.2020.1757711.
[34] A. Swami, J. M. Mendel, and C. L. Nikias, *Higher-Order Spectral Analysis Toolbox for Use With MATLAB*. Natick, MA, USA: The Mathworks Inc., 1995.
[35] W. Bolton, "Alternating current," in *Engineering Science*, 6th ed. Abingdon, U.K.: Routledge, 2021, pp. 177–188, doi: 10.4324/9781315737973-19.
[36] R. Wunenburger, N. Mujica, and S. Fauve, "Experimental study of the Doppler shift generated by a vibrating scatterer," *J. Acoust. Soc. Amer.*, vol. 115, no. 2, pp. 507–514, Feb. 2004, doi: 10.1121/1.1635414.
[37] C. J. Li, J. Ma, and B. Hwang, "Bearing condition monitoring by pattern recognition based on bicoherence analysis of vibrations," *Proc. Inst. Mech. Eng., C, J. Mech. Eng. Sci.*, vol. 210, no. 3, pp. 277–285, May 1996.
[38] I. M. Howard, "Higher-order spectral techniques for machine vibration condition monitoring," *Proc. Inst. Mech. Eng., G, J. Aerosp. Eng.*, vol. 211, no. 4, pp. 211–219, Apr. 1997, doi: 10.1243/0954410971532622.
[39] G. Tacchino, S. Coelli, P. Reali, M. Galli, and A. M. Bianchi, "Bicoherence interpretation in EEG requires signal to noise ratio quantification: An application to sensorimotor rhythms," *IEEE Trans. Biomed. Eng.*, vol. 67, no. 9, pp. 2696–2704, Sep. 2020, doi: 10.1109/TBME.2020.2969278.
[40] C. Soares, *Gas Turbines: A Handbook of Air, Land and Sea Application*. Oxford, U.K.: Butterworth-Heinemann, 2015.

UMAIR AHMED received the bachelor's degree in avionics from the National University of Science and Technology, Islamabad, Pakistan, and the master's degree in avionics from Air University, Islamabad. He is currently pursuing a Ph.D. degree with Cranfield University. He has been working with IVHM Centre, since 2019. He has worked on the development of flight simulators for a period of four years. His role, being a Design Engineer, has been to design and develop software/hardware for integrating various sub-systems of a simulator. For three years, he has also been part of the Aviation Design Institute, where he was tasked to evaluate and integrate various avionics sub-systems. His current research interests include the development of acoustic signal processing and machine learning techniques for fault detection of aircraft auxiliary power unit.

FAKHRE ALI received the degree in mechanical engineering and the Ph.D. degree (engineering) in aerospace propulsion from Cranfield University, U.K. He is currently a Research Fellow of simulation and test with the IVHM Centre, Cranfield University. In his current role, he is responsible for the successful planning, implementation, and delivery of TRL four to five level projects, dedicated to identifying new IVHM solutions for various major civil aircraft sub-systems i.e., APU and ECS. He is also a member of IMechE and RAeS.

IAN K. JENNIONS received the degree in mechanical engineering and the Ph.D. degree in CFD from Imperial College London, London. His career spans over 40 years, working mostly for a variety of gas turbine companies. He has worked for Rolls-Royce (twice). He has worked at General Electric and Alstom in a number of technical roles, gaining experience in aerodynamics, heat transfer, fluid systems, mechanical design, combustion, services, and IVHM. In July 2008, he moved to Cranfield University as a Professor and the Director of the newly formed IVHM Centre. The centre is funded by a number of industrial companies, including Boeing, BAE Systems, Thales, Meggitt, MOD, and Alstom Transport. He has led the development and growth of the centre, in research and education, since its inception. The centre offers an IVHM short course each year and has offered an IVHM M.Sc. He is the Editor of five recent SAE books, such as *IVHM: Perspectives on an Emerging Field*, *IVHM: Business Case Theory and Practice*, *IVHM: The Technology*, *IVHM: Essential Reading*, and *IVHM: Implementation and Lessons Learned*. He is the coauthor of the book *No Fault Found: The Search for the Root Cause*. He is the Director of PHM Society, the Vice-Chairperson of SAE's IVHM Steering Group, a Contributing Member of the SAE HM-1 IVHM Committee, a Chartered Engineer, and a fellow of IMechE, RAeS, and ASME. He is on the Editorial Board for the *International Journal of Condition Monitoring*.